Global model and scaling laws for inductively coupled oxygen discharge plasmas

T. H. Chung,[a] H. J. Yoon, and D. C. Seo
Department of Physics, Dong-A University, Pusan 604-714, Korea

(Received 9 September 1998; accepted for publication 24 June 1999)

For inductively coupled oxygen rf discharge plasmas, a global model which consists of the energy and particle balance equations is formulated. The energy balance equation includes energy losses for electron-neutral elastic collision, excitation, ionization, dissociation, pair production, and charged particle wall loss. Particle balance equations are written for all species of interest. For a specified discharge length and diameter, absorbed power, pressure, electron temperature-dependent reaction rate coefficients and surface recombination constants, we solve these equations to determine the densities of all species and the electron temperature. We measure these parameters by the Langmuir probe method. According to the prevailing particle loss mechanism, the parameter space can be divided into a volume recombination-loss-dominated region and an ion-flux-loss-dominated region. Based on the global model equations, the scaling laws of plasma variables with the control parameters for the ion-flux-loss-dominated region are estimated and compared with the experimental results. © *1999 American Institute of Physics.* [S0021-8979(99)04019-0]

I. INTRODUCTION

Electronegative gases such as oxygen have found numerous applications in plasma processing such as thin-film etching and deposition. The presence of negative ions complicates the discharge phenomena. The number of equations governing the equilibrium is large and analysis becomes difficult.[1,2] There have been many approaches to describe the electronegative plasma. Fluid models have been developed for chlorine gas by Park and Economou[3] and by Sommerer and Kushner.[4] However, fluid models have some limitations in keeping track of the various interacting species since they take considerable computational resources. Spatially averaged global models have also been developed for various regimes of rf discharge plasmas,[1,2,5,6] and analytic equilibrium models have been proposed and compared with the experimental results and other simulation results.[7,8]

In a previous study we developed a two-dimensional fluid simulation to treat an electronegative plasma in a parallel-plane discharge when a single positive ion species is important.[9] There we considered three fluid components (positive and negative ions, and electron). In many electronegative plasmas, more than one positive or negative ion species may be important.

There is an increased demand to understand the scaling of the plasma constituents with control parameters for such multicomponent systems. The scaling of plasma variables (charged particle densities, sheath width, electron temperature, and plasma potential) with the operating parameters gives useful information for the design and analysis of plasma sources. Although the global model does not describe the spatial distribution of charged particles, it should preserve the essential scalings of plasma parameters with control parameters.[5]

Up to now, several attempts to analyze discharge plasmas based on the global model have been made, but those were restricted to the low pressure case[1,2] or the high pressure capacitively coupled case.[5] This study intends to obtain the scaling formulas explicitly throughout the entire range of operating regions, especially around the transition region, and to verify the scaling relations experimentally. Since the scaling itself depends on the operating regions, a division of the parameter space is needed.

In deriving the scaling formulas, we determine the prevailing particle loss mechanism (recombination-loss-dominated or ion-flux loss-dominated). The control parameter space consists of parameters, pL (pressure times system length), and n_eL (electron density times system length). We classify operating regions in the entire control parameter space.[10] In various regions, the discharge generally exhibits different scalings of the operating parameters.

The main purpose of this work is to study scaling features of oxygen rf discharges, and thereby to estimate the influence of operating parameters (neutral gas pressure, applied rf power) on the densities of the charged species and the electron temperature in the discharge and then to compare with the experiment. This article is organized as follows: in Sec. II, a physical model and basic equations are presented; in Sec. III, the scaling laws of plasma variables with the operating parameters are derived. Section IV describes the experimental apparatus and Langmuir probe diagnostics. Section V presents the results of the global model in comparison with the experiment, and discussions, and in Sec. VI, conclusions are summarized.

II. PHYSICAL MODEL AND BASIC EQUATIONS

The reactions considered in this model are

$$e + O_2 \rightarrow O_2^+ + 2e \quad \text{(ionization 2)}$$

$$\{K_{iz2} = 9 \times 10^{-16} T_e^2 \exp(-12.6/T_e)\}, \tag{1}$$

[a]Electronic mail: thchung@plasma.donga.ac.kr

$$e+O_2 \rightarrow O^- + O \text{ (dissociative attachment)} \quad \{K_{att} = 8.8\times 10^{-17}\exp(-4.4/T_e)\}, \tag{2}$$

$$O_2^+ + O^- \rightarrow O_2 + O \text{ (recombination 2)} \quad \{K_{rec2} = 1.5\times 10^{-13}(300/T_g)^{0.5}\}, \tag{3}$$

$$O^- + O^+ \rightarrow 2O \text{ (recombination 1)} \quad \{K_{rec1} = 2.5\times 10^{-13}(300/T_g)^{0.5}\}, \tag{4}$$

$$e+O^- \rightarrow O+2e \text{ (detachment)} \quad \{K_{det} = 2\times 10^{-13}\exp(-5.5/T_e)\}, \tag{5}$$

$$e+O_2 \rightarrow O^- + O^+ + e \text{ (pair production)} \quad \{K_{pair} = 7.1\times 10^{-17} T_e^{0.5}\exp(-17/T_e)\}, \tag{6}$$

$$e+O_2 \rightarrow O+O^+ + 2e \text{ (dissociative ionization)} \quad \{K_{disiz} = 5.3\times 10^{-16} T_e^{0.9}\exp(-20/T_e)\}, \tag{7}$$

$$e+O \rightarrow O^+ + 2e \text{ (ionization 1)} \quad \{K_{iz1} = 9\times 10^{-15} T_e^{0.7}\exp(-13.6/T_e)\}, \tag{8}$$

$$e+O_2 \rightarrow 2O+e \text{ (dissociation)} \quad \{K_{diss} = 4.2\times 10^{-15}\exp(-5.6/T_e)\}, \tag{9}$$

$$O^+ \rightarrow O \text{ (wall recombination)}, \tag{10}$$

$$O_2^+ \rightarrow O_2 \text{ (wall recombination)}, \tag{11}$$

$$O+O \rightarrow O_2 \text{ (wall recombination)}. \tag{12}$$

The metastable species are not included. The energy levels of the metastable oxygen molecule and atom are typically low (e.g., 1 eV), so their contributions via stepwise ionization are quite low. Therefore, the effect of metastable species are neglected for the parameter region we examine.[2] In constructing a global (spatially averaged) model, we assume that the spatial profiles of the charged and neutral particles are flat with their average values, and that the charged particles have very small sheath regions.

From these reactions above, the rate equations for the spatially averaged charged particle densities (the symbol [ ] are used) are written as

$$\frac{d[e]}{dt} = K_{disiz}[O_2][e] - K_{att}[O_2][e] - O_{2\,Loss}^+[O_2^+] + K_{det}[O^-][e] + K_{iz2}[O_2][e] + K_{iz1}[O][e] - O_{Loss}^+[O^+] - \frac{S_p}{V}[e], \tag{13}$$

$$\frac{d[O_2^+]}{dt} = K_{iz2}[O_2][e] - K_{rec2}[O_2^+][O^-] - O_{2\,Loss}^+[O_2^+] - \frac{S_p}{V}[O_2^+], \tag{14}$$

$$\frac{d[O^-]}{dt} = K_{att}[O_2][e] - K_{rec2}[O_2^+][O^-] + K_{pair}[O_2][e] - K_{det}[O^-][e] - K_{rec1}[O^-][O^+], \tag{15}$$

$$\frac{d[O^+]}{dt} = K_{pair}[O_2][e] + K_{disiz}[O_2][e] + K_{iz1}[O][e] - K_{rec1}[O^-][O^+] - O_{Loss}^+[O^+] - \frac{S_p}{V}[O^+]. \tag{16}$$

The particle balance for the neutral species are written as

$$\frac{d[O_2]}{dt} = \frac{Q_{fs}}{V} - (K_{iz2}+K_{att}+K_{diss}+K_{pair}+K_{disiz})[O_2][e] + K_{rec2}[O_2^+][O^-] + O_{2\,Loss}^+[O_2^+] + \frac{1}{2}O_{Loss}[O] - \frac{S_p}{V}[O_2], \tag{17}$$

$$\frac{d[O]}{dt} = K_{att}[O_2][e] + K_{rec2}[O_2^+][O^-] - O_{Loss}[O] + O_{Loss}^+[O^+] + 2K_{diss}[O_2][e] + K_{disiz}[O_2][e] + K_{det}[O^-][e] - K_{iz1}[O][e] + 2K_{rec1}[O^-][O^+] - \frac{S_p}{V}[O]. \tag{18}$$

The energy balance equation can be written as

$$\frac{d(\frac{3}{2}[e]T_e)}{dt} = \frac{P_{abs}}{V} - \varepsilon_{c2}K_{iz2}[O_2][e] - O_{2\,Loss}^+(\varepsilon_e+\varepsilon_i)\times[O_2^+] - (K_{diss}\varepsilon_{diss}+K_{pair}\varepsilon_{pair} + K_{disiz}\varepsilon_{disiz})[e][O_2] - O_{Loss}^+(\varepsilon_e+\varepsilon_i)[O^+] - \varepsilon_{c1}K_{iz1}[O][e]. \tag{19}$$

The collisional energy loss can be expressed as

$$K_{iz2}\varepsilon_{c2} = K_{iz2}\varepsilon_{iz2} + \sum K_{exc2}\varepsilon_{exc2} + K_{el2}\varepsilon_{el2}, \qquad K_{iz1}\varepsilon_{c1} = K_{iz1}\varepsilon_{iz1} + \sum K_{exc1}\varepsilon_{exc1} + K_{el1}\varepsilon_{el1}, \tag{20}$$

where the ε_j terms are the threshold energies required for the processes of ionization, excitation, and elastic collision. The energies of the escaping ions and electrons, and the plasma potential are

$$\varepsilon_i = \frac{T_e}{2} + V_s, \quad \varepsilon_e = 2T_e, \quad V_s = \frac{T_e}{2}\ln\left(\frac{M_{O_2}}{2\pi m}\right). \tag{21}$$

The wall loss rates for neutral atom and charged ions are modeled as

$$O_{Loss} = \gamma_{rec}\frac{v_{th}A}{4V}, \quad O_{Loss}^+ = \frac{u_{BO^+}}{d_{eff}}, \quad O_{2\,Loss}^+ = \frac{u_{BO_2^+}}{d_{eff}}, \tag{22}$$

where γ_{rec} is the surface recombination rate, v_{th} is the thermal velocity of the neutral atom, $A = 2\pi R^2 + 2\pi RL$, $V = \pi R^2 L$, u_{BO^+} and $u_{BO_2^+}$ are the Bohm velocities of oxygen atom and molecule, and the effective system length is

$$d_{\text{eff}}=\frac{R^2L}{2(R^2h_L+RLh_R)}. \tag{23}$$

Note that h_L and h_R are defined as the ratio of the electron density at the bulk to that at the axial sheath and radial sheath respectively.[1,2] If $R\gg L$, Eq. (23) reduces to

$$d_{\text{eff}}\simeq\frac{L}{2h_L}. \tag{24}$$

Here, we use[8]

$$h_L=\left[\frac{a+[u(l)/u_{\text{BO}}]^3}{1+a}\right]^{1/3}, \tag{25}$$

where $a=2\nu_{iz}\lambda/\pi u_{\text{BO}}$, with $\nu_{iz}=K_{iz}n_0$ (n_0 is the neutral particle density), λ is the ion mean free path, $u(l)$ is the velocity of positive ions leaving the electronegative region, and u_{BO} is the average of Bohm velocities of the positive ions. The h_L formula above is derived based on the one-dimensional equilibrium model.[8]

Rewriting Eq. (25) for the adjustment to a spatially averaged global model,[10] we have

$$h_L=\left[\frac{2K_{iz}/\pi\sigma u_{\text{BO}}+(4\nu_{th}\alpha_0/\sigma u_{\text{BO}}n_0l)^3}{1+2K_{iz}/\pi\sigma u_{\text{BO}}}\right]^{1/3}, \tag{26}$$

where σ is the momentum transfer cross section, α_0 is the ratio of the negative ion density to the electron density, and $l\simeq L/2$. In this study, we assume that $h_L\approx h_R$.

The pumping(S_p) and flow(Q_{fs}) rates of neutral species are included to accurately model laboratory situations. In this study, a sinusoidal input power is used.

$$P_{\text{abs}}(t)=P_{\text{abs}}\sin^2(2\pi ft). \tag{27}$$

This model can also be used to study afterglow discharges by turning the power off.[6,11,12]

III. SCALING LAWS

Scaling formulas can be derived providing a dominant positive ion species, and a dominant loss mechanism can be identified. We assume that (1) a steady state is reached, (2) the dominant mechanism of generating ions are the direct ionization of molecules and atoms, (3) for the electron energy balance the collisional energy loss is dominant, (4) $K_{\text{iz2}}\simeq K_{\text{iz1}}, K_{\text{rec2}}\simeq K_{\text{rec1}}$. We note that in reality the positive and negative ion species have approximate parabolic profile or flat-top profile combined with edge parabola along the axis. In this global model, we assume that the average density of the charged species over the spatial distribution is represented as the symbol [ ].

It is known that the abundance of the atomic positive ion, O^+, depends on the surface recombination rate, gas pressure, and absorbed power. For a medium or high pressure discharge plasmas, O_2^+ is the major positive ion, and that the oxygen molecules are far from being completely dissociated, due to a very high oxygen atom recombination frequency on the reactor walls.[13] However, it has been found that the degree of dissociation increases with the rf power. A lower pressure- and higher power-discharges have a larger atomic positive ion density. This study is restricted to lower power discharges.

For the purpose of deriving a simple scaling relations, we set the total positive ion density as $[O_2^+]$. Then, the recombination loss is written as[7,8]

$$\Gamma_{\text{rec}}=K_{\text{rec2}}[O_2^+][O^-]V\simeq K_{\text{att}}[e][O_2]V. \tag{28}$$

The ion loss to the wall is written as[7]

$$\Gamma_{+}=\frac{[e]u_{\text{BO}_2^+}V}{d_{\text{eff}}}. \tag{29}$$

The ratio between these two losses is

$$R_L=\frac{\Gamma_{\text{rec}}}{\Gamma_{+}}=\frac{K_{\text{rec2}}[O_2^+][O^-]d_{\text{eff}}}{u_{\text{BO}_2^+}[e]}\simeq\frac{K_{\text{att}}[O_2]d_{\text{eff}}}{u_{\text{BO}_2^+}}. \tag{30}$$

For a recombination-loss-dominated region ($R_L\gg 1$), the scaling relations of the charged and neutral particle in terms of the control parameters were derived based on a global model for a capacitively coupled discharge.[5] Here, we consider an ion-flux-loss-dominated region ($R_L\ll 1$). Here, the ion-flux loss to the wall is much larger than the volume recombination loss, and the other conditions are the same as those of Ref. 5. The ion-flux-loss-dominated region corresponds to a discharge of low pressure, low power discharge system.[10]

From Eq. (14), if we consider the dominant reactions, we have

$$K_{\text{iz2}}[O_2][e]\simeq O_{2\,\text{Loss}}^+[O_2^+]+K_{\text{rec2}}[O_2^+][O^-]. \tag{31}$$

From Eq. (30), we write

$$K_{\text{rec2}}[O_2^+][O^-]\simeq R_L\frac{u_{\text{BO}_2^+}}{d_{\text{eff}}}[e]. \tag{32}$$

Thus,

$$K_{\text{iz2}}[O_2][e]\simeq\left(1+\frac{R_L[e]}{[O_2^+]}\right)\frac{u_{\text{BO}_2^+}}{d_{\text{eff}}}[O_2^+]. \tag{33}$$

Note that $[e]$ and $[O_2^+]$ are of the same order (or $[O_2^+]$ is greater than $[e]$), and we consider here a small R_L region ($R_L[e]/[O_2^+]\ll 1$).

From the energy balance equation [Eq. (19)],

$$P_{\text{abs}}\simeq V\varepsilon_{c2}K_{\text{iz2}}[O_2][e]+VO_{2\,\text{Loss}}^+(\varepsilon_e+\varepsilon_i)[O_2^+]. \tag{34}$$

Combining Eqs. (33) and (34), we can write

$$P_{\text{abs}}\simeq V(\varepsilon_{c2}+\varepsilon_e+\varepsilon_i)\frac{u_{\text{BO}_2^+}}{d_{\text{eff}}}[O_2^+]. \tag{35}$$

From Eq. (34) and noting that $\varepsilon_L=\varepsilon_{c2}+\varepsilon_e+\varepsilon_i$ is the total electron energy loss, the electron density can be scaled as

$$[e]\propto\frac{P_{\text{abs}}}{pV\varepsilon_LK_{\text{iz2}}}. \tag{36}$$

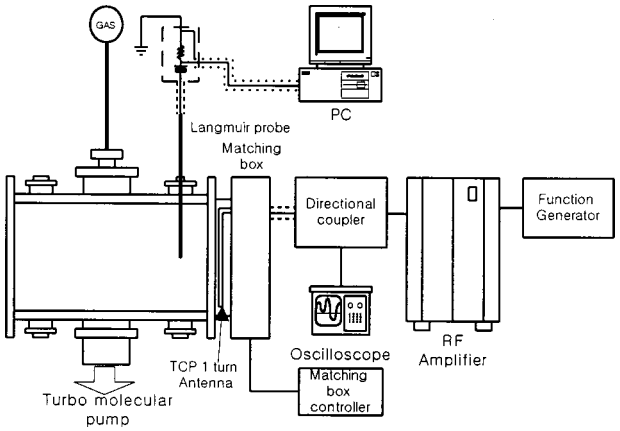

FIG. 1. Schematic of a planar inductively coupled plasma source and Langmuir probe diagnostics system.

Then from Eq. (33),

$$[O_2^+] \approx \frac{d_{\text{eff}} K_{\text{iz2}} [O_2][e]}{u_{BO_2^+}} \propto \frac{d_{\text{eff}} P_{\text{abs}}}{u_{BO_2^+} \varepsilon_L}. \tag{37}$$

As the pressure increases, the electron temperature decreases. Thus, $u_{BO_2^+}$ decreases and K_{iz2} decreases. Since h_L and h_R are found to decrease with the pressure, d_{eff} increases with the pressure. All these factors have nonlinear dependence on the pressure and the power, but $d_{\text{eff}}/u_{BO_2^+}\varepsilon_L$ exhibits an increase with the pressure and are found to be weakly dependent on the power. We also find that in this region (low pressure and low absorbed power) the positive ion and the negative ion have a similar scaling of pressure and power.

Thus, we have a scaling as

$$[O_2^+] \simeq [O^-] \propto p^y P_{\text{abs}}, (y > 0). \tag{38}$$

Note that y depends on the gas composition, operating region, and chamber geometry.

As the pressure further increases, the discharge are in the recombination-loss-dominated region. Then from Eq. (31), $K_{\text{iz2}}[O_2][e] \simeq K_{\text{rec2}}[O_2^+][O^-]$, and assuming $[O_2^+] \simeq [O^-]$, we have

$$[O_2^+] \simeq [O^-] \propto K_{\text{iz2}} P_{\text{abs}}^{1/2}. \tag{39}$$

Therefore we can notice that the positive ion density decreases slightly with increasing pressure in the recombination-loss-dominated region since K_{iz2} decreases with pressure.

IV. EXPERIMENT

The plasma chamber consists of a stainless steel cylinder with diameter 30 cm and length 50 cm. A 1.9 cm thick by 27 cm diameter quartz plate mounted on the one end separates the planar one-turn induction coil from the plasma. Figure 1 shows a schematic of the planar inductive plasma source and Langmuir probe diagnostics system.

The diagnostic port is in the one fourth point to the quartz plate along the cylinder axis. The plasma chamber is evacuated by a turbomolecular pump which has a pumping speed 600 l/s backed by rotary pump giving a base pressure of about $5-8\times10^{-6}$ Torr. The equilibrium gas pressure in the chamber is monitored with a cold cathode gauge. To further control the chamber pressure the gate valve was manually adjusted to vary the pumping speed. The oxygen gas pressure was varied in the range 1–80 mTorr.

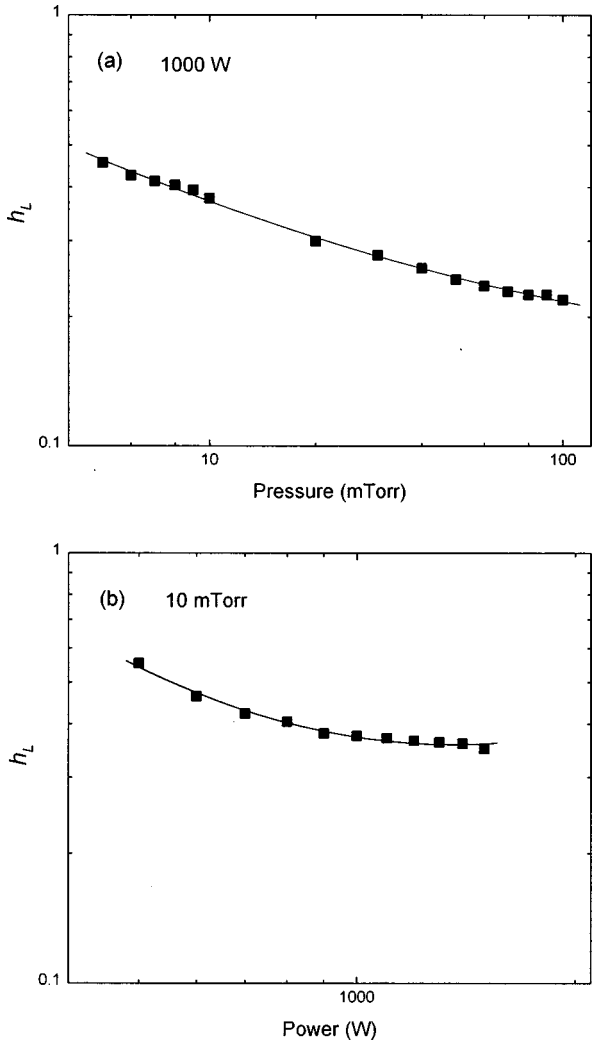

FIG. 2. The variation of h_L as a function of the pressure (a), and the absorbed power (b). $\gamma_{\text{rec}} = 0.1$.

The induction coil is made of copper (without water cooling) and connected to a L-type capacitive matching network, a directional coupler (Amplifier Research DC2600), and a power amplifier (ENI A-500) driven by a function generator (Thander TG2002). A disk-type Langmuir probe is used in the experiment to measure the positive ion density, electron density, electron temperature, and plasma potential.

Experiments were conducted at several pressures and powers. In order to allow the chamber to reach an equilibrium, the plasma was turned on and allowed to run for an hour before taking any measurements. The results of the Langmuir probe measurements are compared with the scaling laws based on a global model.

The saturated current above the space potential is given by

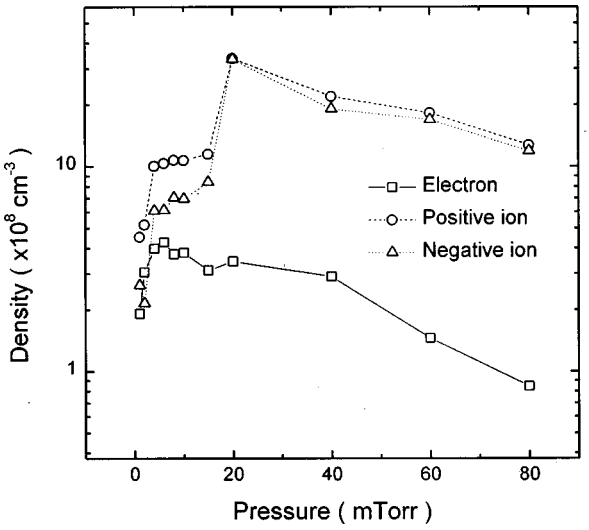

FIG. 3. Measured charged particle densities as a function of the oxygen gas pressure at $P_{abs}=58$ W.

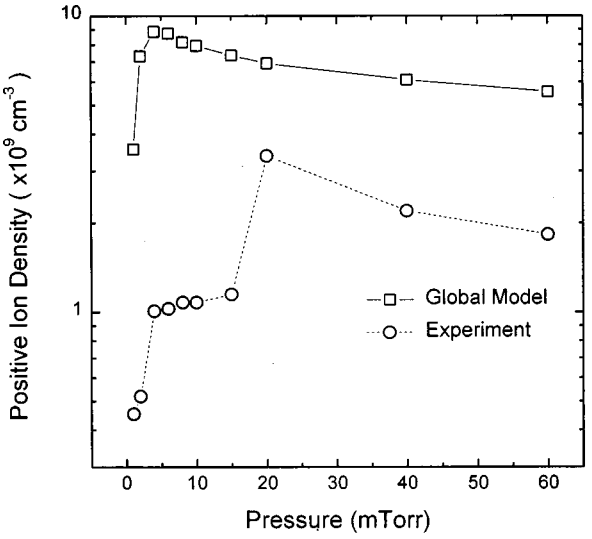

FIG. 4. Comparison in positive ion density between the result of the global model and the experiment.

$$i_s = eS\left[n_e \left(\frac{T_e}{2\pi m} \right)^{1/2} + n_- \left(\frac{T_-}{2\pi M_-} \right)^{1/2} \right], \tag{40}$$

where e is the electronic charge, S is the probe area, n_e is the electron density, m and M_- are masses of electrons and negative ions respectively, T_e and T_- are temperatures of electrons and negative ions, respectively.

The positive ion saturation current is

$$i_+ = 0.6eSn_+ \left(\frac{T_e}{M_+} \right)^{1/2}, \tag{41}$$

where n_+ is the positive ion density and M_+ is the positive ion mass. We have density balance between negatively and positively charged particles given by $n_e + n_- = n_+$. By measuring electron and positive ion saturation currents and the slope of the probe $i-V$ curve, one can obtain the densities of electrons, negative ions, positive ions, and the electron temperature.[14] The ratio of T_e to $T_-(\simeq T_+)$ is assumed to be 50. To determine this ratio more accurately, one has to use a separate double probe along with the single probe.[15]

V. RESULTS AND DISCUSSION

Using the simulation based on the global model equations presented in Sec. II, the effects of the gas pressure and the input power on the charged particle densities and electron temperature are investigated. For a sample calculation, $S_p = 400$ l/s, $Q_{fs}=40$ sccm are used.

In Fig. 2, calculated h_L factor is shown as a function of pressure and absorbed power. As theory predicts,[8] h_L decreases with pressure and power. Therefore, d_{eff} of Eq. (23) increases with pressure as was stated beforehand.

Figure 3 shows the results obtained from Langmuir probe measurements done at $P_{abs}=58$ W for different pressures. The absorbed power is obtained by subtracting the power consumed by the antenna coil and the matching system from the input power. The electron density, the positive ion density, and the negative ion density are measured as a function of the pressure. In this experiment, we can note that the transition from ion-flux-loss-dominated region to recombination-loss-dominated region takes place at about 20 mTorr. Below $p=20$ mTorr (ion-flux-loss-dominated region), the positive and negative ion densities increase with pressure according to Eq. (38), after that, they decrease slightly according to Eq. (39). This can be accounted for from that at medium or higher pressures, the electron detachment and neutral atom detachment become dominant, thus negative ion density decreases. The behavior of the ratio of negative ion to electron density is qualitatively consistent with the experimental results by Tuszewski[16] and Gudmundsson.[17] The ratio increases with increasing pressure. The variation of positive ion density with pressure is also in agreement with the experimental results.[18–20]

Figure 4 shows the comparison between the results of the global model and the experimental results. The model gives an overestimated particle density, and we can note that the transition point is around less than 10 mTorr. However, if we use a higher ratio of electron temperature to negative ion temperature in Eq. (40), we can obtain larger charged particle densities approaching the calculated values.

Figure 5 shows an acceptable agreement between the experimental results of the electron temperature which indicates a decrease and the results of the global model. The prediction of the electron temperature being a weak function of the absorbed power is also confirmed by the experimental measurements (not shown in the figure).

In Fig. 6, the calculated and measured positive ion densities are shown with varying absorbed power. The experimental results are obtained from measurements done at $p=10$ mTorr for different powers. Although the global model produces an overestimated values, both results have similar slopes and are consistent with the scaling formulas within the acceptable limit. Although not shown in the figure, the behavior of the ratio of the negative ion to electron density is qualitatively consistent with the experimental results by

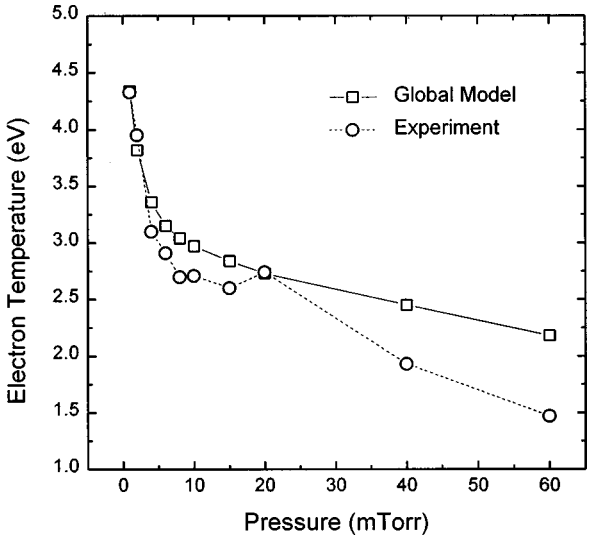

FIG. 5. Measured and calculated electron temperature at $P_{abs}=58$ W.

Tuszewski[16] and Gudmundsson.[17] The ratio decreases with increasing power.

The discrepancy of the order of the magnitude between the calculation and the measurement in Figs. 4 and 6 may be due to the underestimation of sheath potential, V_s in Eq. (21). The absorbed power of 58 W does not guarantee that the discharge is inductive. A capacitive mode makes the sheath potential very high and causes the calculated charged particle densities to be reduced by an order of magnitude. Then the global model is in fair agreement with the experimental data. However, the experimental determination of the plasma potential with respect to the grounded wall excludes the possibility that the discharge is fully capacitive. In reality, the discharge seems partly inductive and partly capacitive, which causes the discrepancy between the calculation based on inductive mode and the measurement.

More accurate descriptions of h_L and h_R factor for electronegative discharges should be included in a further study. A hybrid model which combines the global balance with a consideration of the one-dimensional profiles of the charged particles could provide a better results.[21,22] In addition, the more elaborate techniques including mass spectrometer differentiating O_2^+ and O^+, optical emission spectroscopy are needed to investigate the scaling relations of oxygen atom and atomic ion.

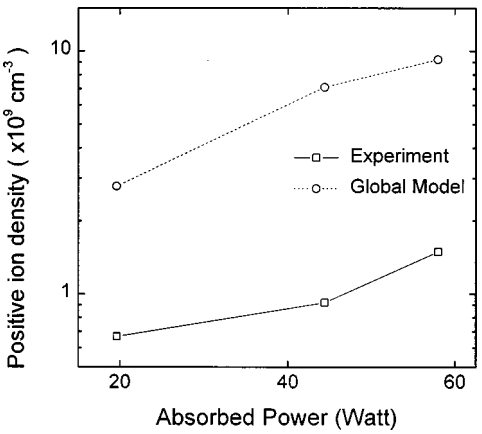

FIG. 6. Measured and calculated positive ion densities as a function of the absorbed power at 10 mTorr.

VI. CONCLUSION

The electronegative inductively coupled oxygen rf discharges have been simulated based on a spatially averaged global model and the results are compared with the experimental results. The charged particle densities and the electron temperature are calculated as a function of the gas pressure and the absorbed power, and are measured by the Langmuir probe method.

They are in agreement overally with each other except that the global model predicts more or less overestimated quantities of the charged particle densities. If a dominant positive ion species and dominant mechanisms of the generation and loss are identified, the global model equations can be used to estimate the scaling laws.

We observe that there exists a transition from a ion-flux-loss-dominated region to a recombination-loss-dominated region. Each region has a different scaling of plasma variables, which proves to be in a good qualitative agreement with the predictions of various models (the one-dimensional equilibrium model and the global model).

The experimental results will be compared to the results of fluid simulation and particle-in-cell simulation wherever possible in a subsequent study. Dependences of charged particle densities on the plasma reactor configurations (target area and cylinder length) should be investigated further by more detailed analysis and experiments. Mass analysis such as quadrupole mass spectrometer is needed to investigate the scaling relations in the discharge in a more detailed manner. The experiments in which a high power rf source and a double probe to measure the accurate value of the ratio of electron temperature to negative ion temperature are being performed to verify these scalings more precisely and to explore the scaling relations at broader operating regions.

ACKNOWLEDGMENTS

We are grateful to Professors A. J. Lichtenberg and M. A. Lieberman of the University of California at Berkeley for fruitful discussions. This work is supported by Dong-A University, Korea Research Foundation Grant No. BSRI-98-2439, Grant No. 1998-001-D00264, Hanbit User Program of Korea Basic Science Institute.

[1] C. Lee and M. A. Lieberman, J. Vac. Sci. Technol. A **13**, 368 (1995).
[2] C. Lee, D. B. Graves, M. A. Lieberman, and D. W. Hess, J. Electrochem. Soc. **141**, 1546 (1994).
[3] S. K. Park and D. J. Economou, J. Appl. Phys. **68**, 3904 (1990).
[4] T. J. Sommerer and M. J. Kushner, J. Vac. Sci. Technol. B **10**, 2179 (1992).
[5] Y. T. Lee, M. A. Lieberman, A. J. Lichtenberg, F. Bose, H. Baltes, and R. Patrick, J. Vac. Sci. Technol. A **15**, 113 (1997).
[6] M. A. Lieberman and S. Ashida, Plasma Sources Sci. Technol. **5**, 145 (1996).
[7] A. J. Lichtenberg, V. Vahedi, M. A. Lieberman, and T. Rognlien, J. Appl. Phys. **75**, 2339 (1994).
[8] I. G. Kouznetsov, A. J. Lichtenberg, and M. A. Lieberman, Plasma Sources Sci. Technol. **5**, 662 (1996).

[9] T. H. Chung, L. Meng, H. J. Yoon, and J. K. Lee, Jpn. J. Appl. Phys., Part 1 **36**, 2874 (1997).
[10] A. J. Lichtenberg, M. A. Lieberman, I. G. Kouznetsov, and T. H. Chung, Plasma Sources Sci. Technol. (submitted).
[11] S. Ashida and M. A. Lieberman, Jpn. J. Appl. Phys., Part 1 **36**, 854 (1997).
[12] M. Meyyapan, J. Vac. Sci. Technol. A **14**, 2122 (1996).
[13] A. Granier, F. Nicolazo, C. Vallee, A. Goullet, G. Turban, and B. Grolleau, Plasma Sources Sci. Technol. **6**, 147 (1997).
[14] H. Amemiya, J. Phys. Soc. Jpn. **57**, 887 (1988).
[15] H. Amemiya, Jpn. J. Appl. Phys., Part 2 **27**, 2423 (1988).
[16] M. Tuszewski, J. Appl. Phys. **79**, 8967 (1996).
[17] J. T. Gudmundsson, Ph.D thesis, University of California at Berkeley, 1996.
[18] J. H. Keller, J. C. Forster, and M. S. Barns, J. Vac. Sci. Technol. A **11**, 2487 (1993).
[19] Y. Ra and C. H. Chen, J. Vac. Sci. Technol. A **11**, 2158 (1996).
[20] M. S. Barnes, J. C. Forster, and J. H. Keller, Appl. Phys. Lett. **62**, 2622 (1993).
[21] T. H. Chung, J. Korean Phys. Soc. **34**, 24 (1999).
[22] H. J. Yoon and T. H. Chung, J. Korean Phys. Soc. **34**, 29 (1999).